PCCP

PAPER

ROYAL SOCIETY OF CHEMISTRY

View Article Online
View Journal | View Issue

Check for updates

Toward a molecular understanding of the conductivity of lithium-ion conducting polyanion polymer electrolytes by molecular dynamics simulation†

Haiming Hua,[a] Boyang Huang,[a] Xueying Yang,[b] Jun Cheng, ✱[c] Peng Zhang✱[b] and Jinbao Zhao ✱[ab]

With the improved lithium-ion transference number near unity, the low conductivity of single lithium-ion conducting solid polymer electrolytes (SLIC-SPEs) still hinders their application in high-rate batteries. Though some empirical conclusions on the conducting mechanism of SLIC-SPEs have been obtained, a more comprehensive study on the quantitative relationship between the molecular structure factors and ionic conduction performance is expected. In this study, a model structure that contains adjustable main chain and anion groups in the polyethylene oxide (PEO) matrix was used to clarify the influence of molecular structural factors on ionic conductivity and electrochemical stability of SLIC-SPEs. The anionic group was further disassembled into the intermediate group and end group while the main chain structure was distinguished into different degrees of polymerization and various lengths of the spacers between anions. Therefore, a well-defined molecular structure was employed to describe its relationship with ionic conductivity. In addition, the dissociation degree of salts and mobility of ions changing with the molecular structure were also discussed to explore the fundamental causes of conductivity. It can be concluded that the anion group affects the conductivity mainly *via* the dissociation degree, while the main chain structure impacts the conductivity by both dissociation degree and mobility.

Received 16th May 2023,
Accepted 11th October 2023

DOI: 10.1039/d3cp02225k

rsc.li/pccp

1. Introduction

Lithium-ion batteries (LIBs) have revolutionized the modern world over the past two decades, playing an essential role in daily life. However, the growing need for a cleaner energy system, such as electric vehicles and large-scale energy storage, poses greater challenges in terms of improving the safety and energy density. To address these challenges, replacing liquid electrolytes with solid polymer electrolytes (SPEs) is an effective

strategy,[1] particularly when paired with a lithium metal anode as it provides the highest theoretical specific capacity.[2] Among the various types of SPEs, one promising strategy involves replacing isolated lithium salts with polyanionic lithium salts to create so-called single lithium-ion conducting solid polymer electrolytes (SLIC-SPEs). In SLIC-SPEs, only lithium ions are capable of long-range migration under the influence of an electric field, leading to higher lithium-ion transference numbers and reduced concentration polarization. These advantages can suppress the growth of lithium dendrites and the adverse reactions of anions with electrodes or current collectors, slowing the deterioration of battery performance.[3–5] Various SLIC-SPEs have been synthesized with different anionic groups, including carboxylates,[6–9] sulfonates,[10–14] sulfonimides,[15–23] and boric acid esters.[24–30] Generally, practical SLIC-SPEs contain polymer solvents, such as polyethylene oxide (PEO),[19,22,31] to facilitate the dissociation of "free" lithium ions, which play a leading role in lithium transport. Despite this, the production of "free" lithium ions is impeded by the strong electrostatic forces between lithium ions and fixed anionic groups, resulting in a low ionic conductivity in SLIC-SPEs.

There are two common strategies to improve the conductivity of SLIC-SPEs. One is to enlarge the delocalization structure

[a] College of Chemistry and Chemical Engineering, State-Province Joint Engineering Laboratory of Power Source Technology for New Energy Vehicle, State Key Laboratory of Physical Chemistry of Solid Surfaces, Engineering Research Center of Electrochemical Technology, Ministry of Education, Collaborative Innovation Center of Chemistry for Energy Materials, Xiamen University, Xiamen 361005, Fujian, China. E-mail: jbzhao@xmu.edu.cn

[b] College of Energy, Xiamen University, Xiamen 361102, Fujian, China. E-mail: pengzhang@xmu.edu.cn

[c] State Key Laboratory of Physical Chemistry of Solid Surfaces, Collaborative Innovation Center of Chemistry for Energy Materials (iChEM), MOE Key Laboratory of Spectrochemical Analysis and Instrumentation, College of Chemistry and Chemical Engineering, Xiamen University, Xiamen, China. E-mail: chengjun@xmu.edu.cn

† Electronic supplementary information (ESI) available. See DOI: https://doi.org/10.1039/d3cp02225k

29894 | *Phys. Chem. Chem. Phys.*, 2023, **25**, 29894–29904

This journal is © the Owner Societies 2023

Published on 12 October 2023. Downloaded by Xiamen University on 3/7/2025 9:14:38 AM.

of the anion group by introducing a conjugated system to weaken its interaction with lithium ions. As a type of representative anion group, sulfonimide anion and its many derivatives have been synthesized and studied. For instance, at 90 °C, the conductivity of $-SO_3^-Li^+$, $-[SO_2-N-SO_2-CF_3]^-Li^+$, and $-[SO_2-N-SOCF_3-N-SO_2-CF_3]^-Li^+$ could reach 10^{-7}, 10^{-5}, and 10^{-4} mS cm^{-1}, respectively. It clearly shows that enlarging the conjugated system can increase the conductivity by orders of magnitude as the negative charge is better dispersed.[19] The other strategy is to optimize the structure of the polymer main chain. Compared with the common self-polymerization of lithium salt monomers, the copolymerization of anionic salts and other functional monomers could lead to products with improved conductivity.[32]

Although some progress has been made in understanding the conductance laws of SLIC-SPEs, several unresolved questions still remain and should be answered from a more fundamental perspective. For the structure of anion groups, is there an extreme point as the conductivity enhanced continuously by increasing the size of the conjugated system? How does the main chain structure impact the ionic conductivity? Additionally, how do the structure factors affect the redox stability? Collectively, the answers to these questions are crucial in constructing a full-scale map for the development of SLIC-SPEs. Unfortunately, these questions are difficult to answer by experimental study alone due to the few well-defined molecular structures that could be synthesized. However, computational simulation methods combined with a small amount of validation experiments provide an opportunity for studying these questions efficiently and inexpensively.

Molecular dynamics[8,33-38] (MD) simulations have been widely used to investigate the ion transport properties of liquid electrolytes, inorganic solid electrolytes, and polymer electrolytes. For double ion conductor polymer electrolytes, the diffusion behavior of lithium ions in the PEO matrix has been deeply studied, which accelerates the research and development of polymer electrolytes.[39-42] Notably, PEO is a commonly used polymer solvent[19,22,31] for SLIC-SPEs due to its adequate ether-oxygen distance that allows it to chelate with Li-ions as well as its flexible chain segments, which allow for flexible Li-ion movement with the polymer chains.[43]

In SLIC-SPEs, the variations in the anion groups and main chain structures add a layer of complexity to the prediction of their conductivities. Therefore, it is crucial to carefully identify and study these structural factors. The classical MD method is a cost-effective method for predicting the conductivity of polymer electrolytes as the more accurate *ab initio* molecular dynamics (AIMD) method is too expensive.[44-46] However, the classical force field is deficient in quantitative accuracy when the parameters are not calibrated,[47,48] especially the charge scale factor n_s used to correct the polarization between ions for a better approximation of anion dissociation. In many simulation researches, n_s is determined based on empirical values, leading to the less reliable estimations of conductivities. At the same time, the commonly used approach of obtaining conductivities from the diffusion coefficient by the Nernst–Einstein equation shows poor accuracy for SLIC-SPEs, which contain many undissociated ions.[49,50]

In this work, the conductivities of several lithium salts in short and long chains PEO were measured to optimize the key parameter n_s in MD simulations. PEO was used as a representative polymer solvent here to facilitate the dissociation of lithium ions for the purpose of studying the impact of the polyanion chain structure on the conductivities. To ensure the quantitative accuracy of the conductivity simulation, the electric field drift method, which is more accurate in principle, was used. The influence of the anion structure and main chain structure on the conductivities of SLIC-SPEs were studied using a model contains R1 intermediate group, R2 end group, and R3 main chain (Fig. 1).

In addition, as the dissociation degree of salts (α) and mobility of lithium ions (u) are two important factors of
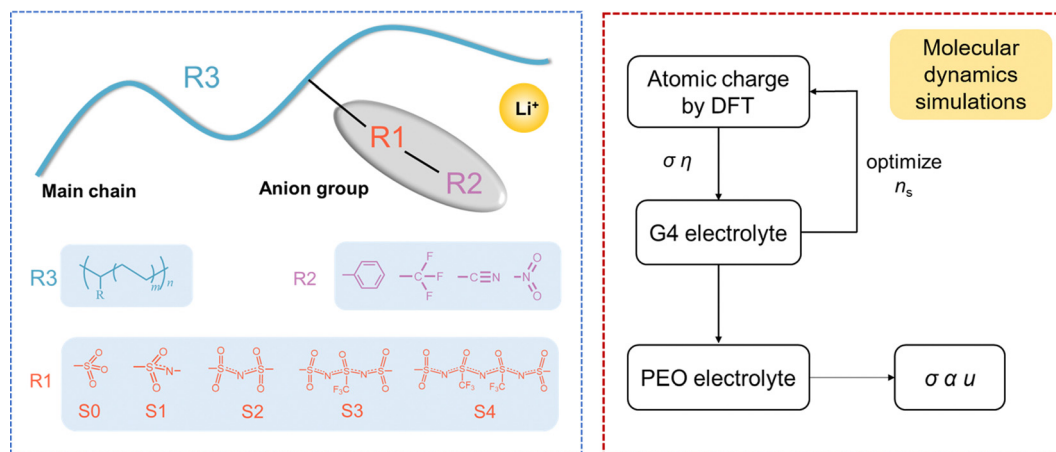
Fig. 1 Left: Schematic diagram of the sulfonimide SLIC-SPEs molecular structure, which consists of different intermediate group factors with various sizes of the conjugated system (R1), end group factor with adjustable electronic effect (R2), and main chain factor with different *n* and *m* (R3). Right: Flow chart for optimizing the parameters of molecular dynamics force field. σ, α, u, and η are conductivity, dissociation degree, mobility, and viscosity, respectively.

This journal is © the Owner Societies 2023

Phys. Chem. Chem. Phys., 2023, **25**, 29894–29904 | **29895**

conductivity (σ) in the definition of conductivity formula 1, α and u were discussed emphatically to explore the underlying causes of conductivity (c is salt concentration, F is Faraday constant). Although decomposing the conductivity into the average dissociation degree and average mobility is an approximation, which does not consider the different speeds of free lithium ions, it still provides a comprehensive analysis of conductivity and establishes a foundation for designing the structures of SLIC-SPEs.

$$\sigma = nqu = \alpha ucF \qquad (1)$$

The results showed that the modification of the anionic group structure primarily influences the conductivity *via* α, while the modification of the main chain structure affects the conductivity through both α and u. In view of the current stage of research on SLIC-SPEs, raising u through a rational design of the polyanion chain is a more promising approach. These findings provide valuable insights into the design of high conductivity SLIC-SPEs. Furthermore, the methods employed in this study offer a theoretical guidance for the structural design of functional polymers.

2. Simulations and experimental methods

2.1. Materials

Lithium bis(trifluoromethane)sulfonimide (LiTFSI) was kindly supplied by Guotaihuarong Co. (China). Lithium (trifluoromethane)sulfonate (LiCF$_3$SO$_3$), lithium trifluoroacetate (LiCF$_3$COO), lithium perchlorate (LiClO$_4$), lithium acetate (LiCH$_3$COO), tetraethylene glycol dimethyl ether (G4), and polyethylene glycol 10 000 (PEG-10 000) were purchased from Energy Chemical Co. (China). Lithium ethylsulfonyl(trifluoromethyl)sulfonimide (LiEtTFSI or LiEt(SO$_2$)N(SO$_2$)CF$_3$) and lithium ethanesulfonate (LiEtSO$_3$) were prepared by organic synthesis (see the ESI†).

All electrolytes were prepared in an inert argon-filled glove box (H$_2$O < 0.1 ppm, O$_2$ < 1 ppm). G4 electrolytes preparation method: the weighed salt was transferred to a 10 mL tube, and 2 mL G4 was then added. The mixture was heated to 80 °C under stirring for 4 h and then left undisturbed after cooling to normal temperature.

PEG-10 000 electrolytes preparation method: weighed ground PEG-10 000 crystal particles were mixed evenly with the weighed salt in a 10 mL glass tube. The mixture was melted at 100 °C under stirring for 8 h and then left undisturbed after cooling to 80 °C.

2.2. Lithium salt synthesis method

The synthesis methods of LiEtSO$_3$ and LiEtTFSI are in the ESI.†

2.3. Measurements

2.3.1. Density measurement. The densities of G4 solutions were measured at 25 °C to verify the simulation results. 0.800 mL solution was transferred with a pipette gun and then weighted on the one over ten-thousand analytical balance.

The mass was measured through weighing five times. After removing the maximum and minimum values, the density (ρ_{exp}) was obtained by calculating the average value of the three results.

2.3.2. Viscosity measurement. A vibrating viscometer (model: SEKONIC VISCOMATE VM-10A series) was used for viscosity measurements at 25 °C.

2.3.3. Ionic conductivity measurement. The conductivities of G4 electrolytes were measured at 25 °C while the conductivities of PEG-10 000 electrolytes were measured at 80 °C. 2 mL electrolyte was put into a 10 mL centrifuge tube and then a bright platinum conductivity electrode was inserted into the tube. The AC impedance data was obtained by a Solartron electrochemical workstation, and the voltage amplitude was 10 mV with the frequency ranging from 10^5 Hz to 1 Hz. The data from 10^4 Hz to 10 Hz were linearly fitted, and then the conductivity σ_{exp} was obtained from formula 5. R_a taken from the real axis intercept of the Nyquist plot is the electrolytic cell resistance. L is the distance between the two platinum electrodes and S is the area of the platinum electrode. The conductivity electrode was purchased from Leici Co. (China). The conductivity cell constant is 1.045 cm^{-1} (corresponds to L/S in formula 5).

$$\sigma = \frac{L}{R_a \cdot S} \qquad (5)$$

2.3.4. Synthetic salt characterization. The AVANCE NEO 500 MHz Digital FT-NMR Spectrometer was used to record the ^{1}H, ^{19}F, and ^{13}C NMR spectra. The synthetic salt was dissolved in DMSO-d$_6$ solutions. Inductively coupled plasma-optical emission spectrometry was used to measure the content of cation ions. The solution containing about 10 mg mL^{-1} Li element was prepared with ultrapure water. The content of lithium ion and potassium ion in the solution was measured to confirm whether the potassium ion was slightly excessive so as to ensure that there was no lithium perchlorate residue in the system to make the conductivity falsely higher.

2.4. Simulation methods

2.4.1. Quantum chemical calculation methods. Gaussian09 E01[51] software package was used to perform quantum chemical calculation. Geometrical optimization and frequency analysis were performed at the B3LYP-D3/6-311+G(d,p)[52–54] theoretical level. Based on the obtained wave function, the restrained electrostatic potential (RESP) atom charges[55] and electrostatic potential (ESP) data were calculated using Multiwfn software.[56,57] The visualization of the molecular structure and ESP were performed by VMD software.[58]

2.4.2. Molecular dynamics simulation methods. MD simulations were performed using Gromacs2018.8 software[59] with OPLS-AA force field,[60,61] which is suitable for the simulation of the solution and polymer.[33,34] Tetraethylene glycol dimethyl ether (G4) was used to represent the model of short chain PEO. G99 with 99 EO structural units was used to represent the

29896 | *Phys. Chem. Chem. Phys.,* 2023, **25**, 29894–29904

This journal is © the Owner Societies 2023

model of the long chain PEO as the conductivity of the PEO electrolyte convergences when the number of structural units is over 90 (molecular weight over 4000).[62,63] Short-chain PEO and long-chain PEO were both used to fully check the accuracy of the MD simulation. As the migration mechanism of lithium ions in short-chain and long-chain PEO is different,[41] while the basic motion forms of them are the same (bond stretching, bond angle bending, dihedral angle rotation). Meanwhile, the experimental data such as density and viscosity in G4 are more accurate as its liquid form at room temperature, and these physical quantities can be used to verify the accuracy of the MD simulation.

The force field and atomic charge of the PEO chain were obtained from the literature.[64] Also, the force field of the anions and polyanion were generated using the Acpype program.[65] In order to easily expand the simulation results to other anions not mentioned in the article, we did not adjust the force field parameters of the anion artificially, although adjusting the force field parameters (especially the dihedral angle parameters) according to the results of quantum chemical calculations will make the simulation results better. RESP atom charges, which could accurately describe the surface electrostatic potential distribution of molecules, were used for the anions. In order to consider the polarization effect between lithium ions and anions, effective atomic charge q_{eff} with several correction factors n_s of 0.70, 0.75, 0.78, or 0.80 was used. $q_{eff} = n_s \cdot q_{RESP}$. Also, the value $n_s = 0.78$, which is the best one (Section 3.1), was used for subsequent calculations.

The simulation boxes were established by Packmol software.[66] For G4 electrolyte solution, the boxes were directly constructed. For the G99 polymer electrolyte, the molecular chain was first heated to melt into a ball and then put into the boxes with anions and lithium ions. The simulation boxes were firstly submitted to energy minimization using the steepest descent method. The equilibrium simulations were carried out under isothermal–isobaric (NPT) ensemble. A time step of 2 fs was used for solving the equation of motion. Berendsen and Velocity-rescale methods were used for pressure coupling and temperature coupling, respectively. The equilibrium simulation was operated for 20 ns at 298.2 K and 1 bar for G4 electrolyte, while it is more challenging to make the boxes in equilibrium than small-molecule liquid systems such as in a G99 electrolyte. Therefore, an annealing method was utilized to accelerate the equilibration of the polymer system. Specifically, the pre-equilibrium simulation was operated for 40 ns at 598.2 K and 1 bar, followed by an annealing process to 353.2 K in 80 ns, and the equilibrium simulation was operated for 40 ns at 353.2 K. The production simulations were carried out under canonical (NVT) ensemble for 40 ns at the same temperature with equilibrium simulations. For the diffusion coefficient calculations of the G99 electrolytes, 200 ns of NVT production simulation was performed.

2.4.3. Simulation of density, viscosity, dissociation degree, and conductivity. Density (ρ_{sim}) was calculated from the last 5 ns of equilibrium simulation. Viscosity (η_{sim}) was calculated by periodic perturbation method[67] with cos-acceleration as 0.05 nm ps^{-2} for 1 ns at 25 °C. Dissociation degree (α) in this work was defined as the average percentage of lithium ions that are not coordinated with anions within 2.4 Å in production simulation. Average mobility (u) was calculated according to formula 1. The radial distribution function (RDF) analysis and cluster size analysis were obtained by Gromacs. In cluster size analysis, any two lithium ions were considered to be in a cluster when the distance between them was less than 0.78 nm.

The simulations of conductivities were performed under NVT ensemble with electric field E. Higher electric field strengths will increase the drift current to reduce relative error but may cause the conductivity to deviate from linearity.[68,69] After a test of several E for four representative systems with different conductivity, namely, LiTFSI, LiEtTFSI, (LiEtTFSI-PE$_4$)$_{11}$, and LiEtSO$_3$ in the G99 electrolyte (Fig. S2, ESI†), the following scheme was selected. $E = 0.05$ V nm^{-1} was used for the monovalent salt in the G4 solution. $E = 0.10$ V nm^{-1} was used for the monovalent salt in the G99 system (Sections 3.1 and 3.2) and $E = 0.20$ V nm^{-1} was used for the polyanionic system (Section 3.3). The conductivity was calculated by formula 2, where v, c, E, Z, F, k, and e are average drift rate, molarity of ion, electric field strength, ion charge, Faraday constant, Boltzmann constant, and elementary charge, respectively. The conductivity obtained by the electric field drift method is recorded as σ_{elec}. v was obtained from the slope of drift curve by least squares method. A drift curve was divided into two equal-length segments to measure the error in conductivity. The relative deviation is expressed as $\pm |v_1 - v_2|/2$ as the slopes of the two curves were obtained as v_1 and v_2, separately.

$$\left. \begin{array}{l} \sigma_{elec+} = \dfrac{v^+}{E} \cdot c^+ \cdot Z^+ \cdot F \\[2mm] \sigma_{elec-} = \dfrac{v^-}{E} \cdot c^- \cdot Z^- \cdot F \\[2mm] \sigma_{elec} = \sigma_{elec-} + \sigma_{elec+} \end{array} \right\} \quad (2)$$

The diffusion coefficient (D) was simulated by mean square displacement (MSD) method in production simulation (formula 3). $r(t)$ is the displacement of the particle at time t, and D was converted into conductivity σ_{diff} by Nernst Einstein eqn (4). For G99 electrolytes, A linearly well-behaved range from 100 ns to 150 ns was used for slope fitting. An MSD curve was divided into two equal-length segments to measure the error in D. The relative deviation is expressed as $\pm |D_1 - D_2|/2$.

$$D = \lim_{t \to \infty} \frac{|r(t) - r(0)|^2}{6t} \quad (3)$$

$$\left. \begin{array}{l} \sigma_{diff+} = D^+ c^+ \dfrac{Z_+^2 eF}{kT} \\[2mm] \sigma_{diff-} = D^- c^- \dfrac{Z_-^2 eF}{kT} \\[2mm] \sigma_{diff} = \sigma_{diff+} + \sigma_{diff-} \end{array} \right\} \quad (4)$$

This journal is © the Owner Societies 2023

Phys. Chem. Chem. Phys., 2023, **25**, 29894–29904 | **29897**

3. Results and discussion

3.1. Determining and checking the scale factors n_s

The accuracy of MD simulation in electrolyte solution depends on the force field parameters, especially atomic charges. σ_{elec} and σ_{exp} of several salts (LiTFSI, LiClO$_4$, LiCF$_3$SO$_3$, LiCF$_3$COO, LiCH$_3$COO, LiEtSO$_3$, and LiEtTFSI) in G4 solution with the O/Li ratio = 20:1 were compared to optimize the scale factors n_s (Section 2.3). These lithium salts contain both commercial lithium salts for LIBs and two model lithium salts, LiEtSO$_3$ and LiEtTFSI. σ_{exp} and σ_{elec} of each n_s (0.70, 0.75, 0.78, and 0.80) are marked in Fig. 2a. Mean squared error (MSE) was used to describe the compliance of σ_{elec} and σ_{exp}. N_s was determined to be 0.78 as σ_{elec} agreed best with the σ_{exp} (MSE = 0.18). Then, the σ_{elec} with O/Li = 50 in G4 solution and the O/Li = 20:1 in G99 solution were simulated using n_s = 0.78 to check this parameter (Fig. 2b). The conductivities showed a good agreement (MSE = 0.02 and 0.07, respectively), such as the densities and viscosities (Table S1, ESI†). The above results showed that the force field parameters and the electric field drift method could well describe the ionic conduction behavior of different lithium salts in the short chain or long chain PEO electrolytes.

For LiTFSI in G4 solution, σ_{elec} = 1.85 mS cm^{-1}, which is lower than σ_{exp} = 2.94 mS cm^{-1}, had a larger deviation compared with other salts (Table S2, ESI†), which may be due to the large flexibility of TFSI anion compared with other rigid anions. The dihedral angle parameters used in the simulation were not adjusted artificially to make the method scalable.

The σ_{diff} calculated from the diffusion coefficient through Nernst Einstein eqn (4) is commonly employed to describe the conductivity behavior of the electrolytes. The reliability of this method in this system was assessed by the comparison of σ_{diff} and σ_{exp}, as shown in Fig. 2c. G4 electrolytes exhibit poor linearity between σ_{diff} and σ_{exp}, while G99 electrolytes display significantly improved linearity. Nonetheless, there are two critical drawbacks that hinder this method from being an accurate predictive tool. Firstly, the order of σ_{diff} does not correspond with σ_{exp}, such as LiTFSI > LiClO$_4$ in σ_{exp}, whereas σ_{diff} presents the opposite trend. Secondly, falsely high σ_{diff} appear in salts with extremely low conductivity. Several factors potentially contribute to the low accuracy of σ_{diff}. For systems in which complete dissolution occurs but with ion pairing (salts excluding LiCH$_3$COO and LiEtSO$_3$), the relationship between

the diffusion coefficient and ionic conductivity deviates from the Einstein equation. This is because the equation assumes all charge carriers are free and contribute equally to ionic conductivity. However, the diffusion of associated ions cannot contribute to ionic conductivity like free ions due to the overall electrical neutrality of the anion–cation clusters.[49,50] Consequently, σ_{diff} are generally higher than the experimental values. For salts that are difficult to dissolve in experiments (LiCH$_3$COO and LiEtSO$_3$), although cations and anions would all form clusters in MD simulation, ions could still diffuse with the clusters owing to the limited size of the simulation box. This non-physical behavior, however, does not occur in reality. If a hypothetical macroscopic simulation box were employed, cations and anions would aggregate into macroscopic clusters, leading to a near-zero diffusion coefficient. Fortunately, the electric field drift method can accurately replicate the near-zero ionic conductivities of these salts as the non-physical diffusion of cations and anions in large clusters is effectively cancelled out. The advantage of the electric field drift method is of great significance as phenomena such as non-dissolution and phase separation may occur in SLIC-SPEs. Therefore, in this work, σ_{elec} was used to investigate the laws governing electric migration.

3.2. Relationship between lithium ion conductivity and anion structure

In SLIC-SPEs, the structure of the anion groups attached to the polymer chain greatly affects the ionic conductivity. In order to conduct a more quantitative and systematic study of the relationship between structures and conductivities, the sulfonimide anion group, which is used most widely, was chosen as the model structure.

The structure of sulfonimide derivatives lithium salts SLIC-SPEs is composed of main chain (R3) and anion group. The anion group can be further split into intermediate group (R1) and end group (R2). The schematic diagram and the groups studied in this work are shown in Fig. 1. The impact of R1 and R2 on the ionic conductivity were discussed in this section with the R3 set as the ethyl chain. It should be pointed out that the variety of R1 and R2 group correspond to the two strategies for designing anionic groups, namely, increasing the size of the conjugated system or changing the electron withdrawing
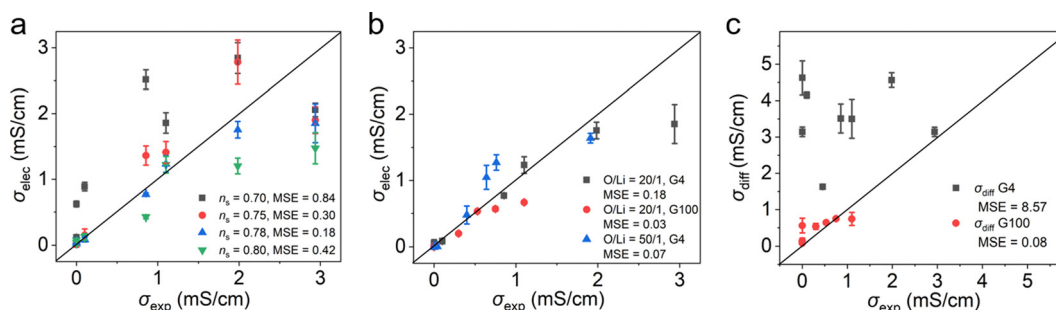
Fig. 2 Relationships between (a) σ_{elec} and σ_{exp} for salts in G4 electrolyte with O/Li = 20:1. (b) σ_{elec} and σ_{exp} for electrolyte with n_s = 0.78. (c) σ_{diff} and σ_{exp} for salts in G4 electrolyte with O/Li = 20:1. MSE is mean squared error.

29898 | *Phys. Chem. Chem. Phys.*, 2023, **25**, 29894–29904

This journal is © the Owner Societies 2023
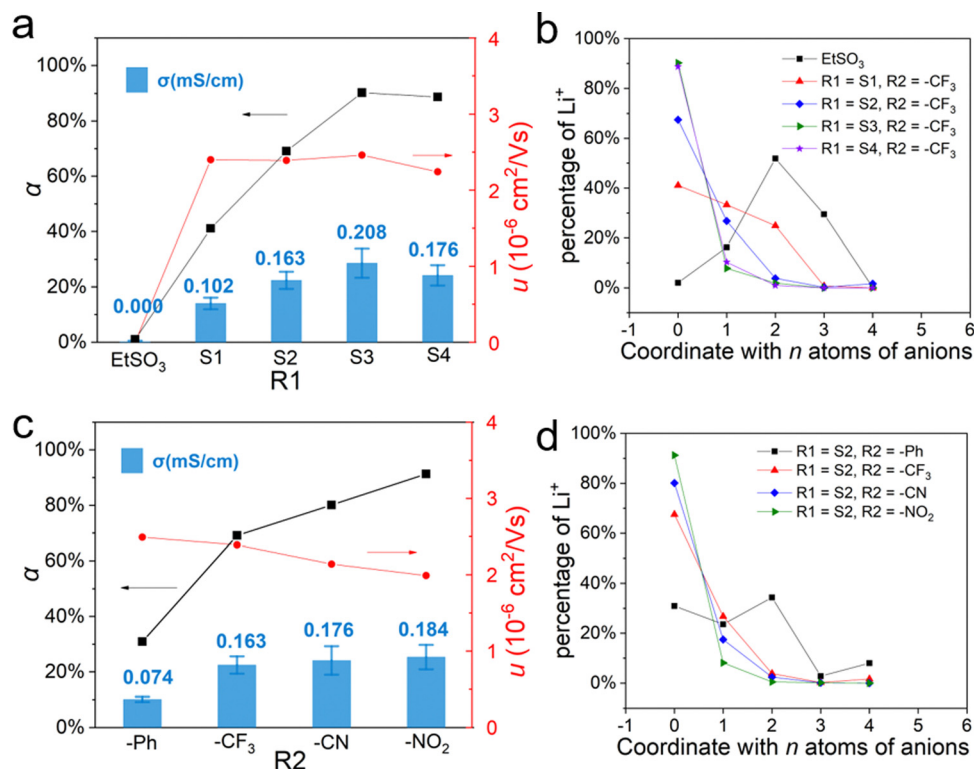
Fig. 3 The simulation results of LiEt-R1-R2 salts in G99 electrolyte with O/Li = 20 at 80 °C. (a) and (c) σ, α, and u of the electrolytes. (b) and (d) Percentage of Li^+ coordinated with N atoms of anions.

groups at the end, respectively. The effects of R1 and R2 were studied separately. σ, α, u, and the coordination situation of lithium ions are shown in Fig. 3. In this section, σ and u represent the conductivity and mobility of lithium ions, respectively. The simulation boxes of these electrolytes are shown in Fig. S7 (ESI†).

When R2 is set as -CF$_3$ and R1 transforms from S0 to S4, the σ of LiEtSO$_3$, LiEt(SO$_2$)NCF$_3$, LiEt(SO$_2$)N(SO$_2$)CF$_3$, LiEt(SO$_2$)N(SOCF$_3$)N(SO$_2$)CF$_3$, and LiEt(SO$_2$)N(SOCF$_3$N)$_2$(SO$_2$)CF$_3$ are 0.000, 0.102, 0.163, 0.208, and 0.176 mS cm^{-1}, respectively, showing that increasing the size of the R1 group significantly increases the σ from S0 to S3, which is consistent with the experimental results.[70,71] However, the σ does not continue to rise from S3 to S4, which shows that the σ does not increase monotonically with the increasing size of the anion group.

When R1 is set as S2 and R2 is –Ph, –CF$_3$, –CN, and –NO$_2$, respectively, the σ of LiEt(SO$_2$)N(SO$_2$)Ph, LiEt(SO$_2$)N(SO$_2$)CF$_3$, LiEt(SO$_2$)N(SO$_2$)CN, and LiEt(SO$_2$)N(SO$_2$)NO$_2$ are 0.074, 0.163, 0.176, and 0.184 mS cm^{-1}, respectively. The sequence of σ is consistent with the electron-withdrawing ability of R2, showing that the increasing electron-withdrawing ability of R2 could improve the σ; however, it clearly can be identified that the impact of the R2 group shows much weaker impact than that of R1. The electron withdrawing ability of the –CF$_3$ group is strong enough for R1 = S2 as the σ can only be slightly improved by replacing –CF$_3$ with much stronger electron withdrawing groups like –NO$_2$.

According to formula 1, α and u are the two determinants of σ. ESP is a method to reflect the charge distribution on the molecular surface. The minimum value of the ESP (ESP$_{min}$) reflects the Coulombic binding of the anion group to the lithium ion, which greatly affects α. The ESP distribution coloring diagrams are shown in Fig. 4a with ESP$_{min}$ being marked on the diagram. To further analyze the essential reasons for the changing trend in conductivity, the α and u of lithium ions and ESP were analyzed.

The trend of α and ESP$_{min}$ is basically the same as that of σ. For R1 = S2 and R2 = –Ph to –NO$_2$, the ESP$_{min}$ changes from -120.2 kcal mol^{-1} to -111.6 kcal mol^{-1}, and α changes from 30.9% to 91.3%. For R2 = –CF$_3$ and R1 = S1 to S4, the ESP$_{min}$ changes from -126.1 kcal mol^{-1} to -93.5 kcal mol^{-1}. α rises firstly from 41.1% to 90.2% for S1 to S3 and then falls down from 90.2% to 88.7% for S3 to S4, which is consistent with σ. The appearance of the turning point is probably because the decrease in the negative charge on the coordination atoms cannot offset the increasing in the number of coordination atoms as the size of R1 increases. U is not the main determinant of σ for the listed sulfonimide salts as it varies a little from 2.0×10^{-6} to 2.5×10^{-6} cm^2 V^{-1} s^{-1}. Therefore, the increase in σ can be mainly attributed to the increase in the α caused by the negative charge distribution on anions.

Besides the ionic conductivity, the electrochemical stability window also plays an important role in the application of polymer electrolytes. The oxidation and reduction resistance of the anions should be taken into consideration as a result.

This journal is © the Owner Societies 2023

Phys. Chem. Chem. Phys., 2023, **25**, 29894–29904 | **29899**
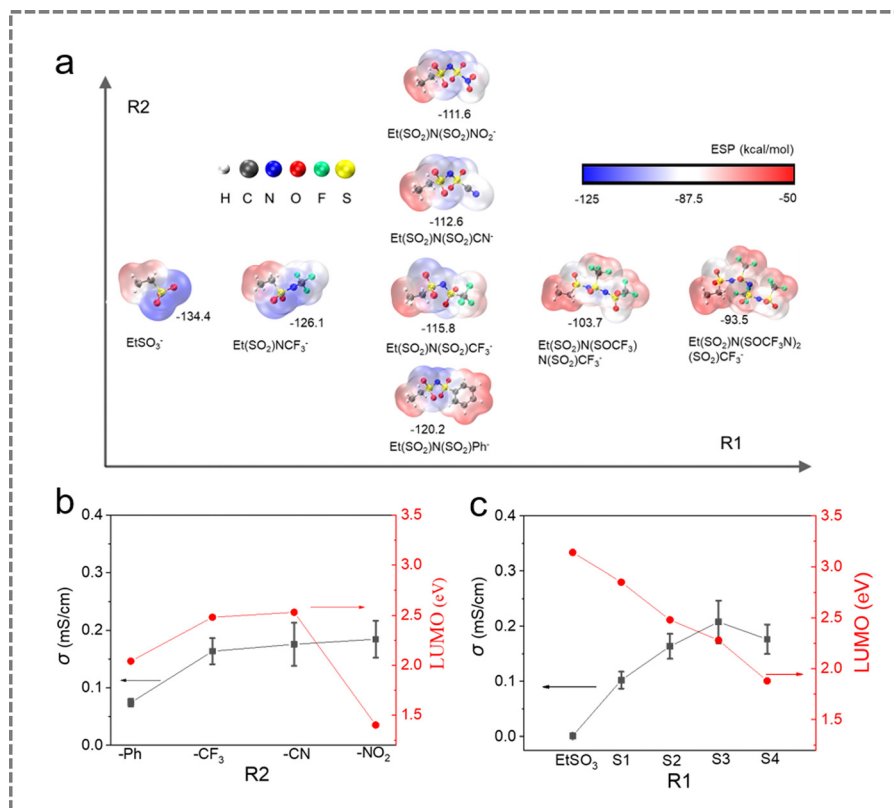
Fig. 4 (a) ESP distribution coloring diagram of sulfonimide anion. ESP$_{min}$ was marked in the corresponding position of the molecule. Theoretical level: B3LYP-D3/6-311+G(d,p). (b) σ and LUMO for different R2 with R1 = $-$CF$_3$. (c) σ and LUMO for different R1 with R2 = S2.

The highest occupied molecular orbital (HOMO) and lowest unoccupied molecular orbital (LUMO) energy levels were calculated to study the oxidation/reduction resistance of these anions as the frontier orbital energy levels are the approximation of oxidation and reduction potential. The results are shown in Table S2 (ESI†) and Fig. 4b and c. It can be concluded that increasing the size of R1 would decrease both the HOMO and LUMO values, making the anions harder to be oxidized but easier to be reduced. As a result, the size of the R1 group should be kept moderate as a lower LUMO means that the anion is prone to side reactions at the negative electrode of the battery.

The effect of R2 is more complex. The HOMO generally decreases with the increase in the electron withdrawing ability. However, for LUMO, inducible effect groups and conjugated effect groups have different influences. For conjugation effect groups like phenyl and nitro, the LUMO values are 2.04 eV and 1.73 eV, respectively. For the inductive effect groups $-$CF$_3$ and $-$CN, the LUMO values are 2.48 eV and 2.53 eV, respectively, higher than that of the former groups, showing that the R2 group with induced electron-withdrawing effect has a stronger resistance to reduction.

3.3. Relationship between lithium ion conductivity and main chain structure factor

The main chain structure factor R3 (Fig. 2) is also an important one affecting the conductivity of SLIC-SPEs. The general formula of the model structure for changing the main chain is (LiEtTFSI-PE$_m$)$_n$. LiEt(SO$_2$)N(SO$_2$)CF$_3$ (LiEtTFSI) is employed as it is a commonly used anionic group with high conductivity. In order to investigate the effect of polymerization, (LiEtTFSI)$_2$, (LiEtTFSI)$_4$, and (LiEtTFSI)$_{11}$ were constructed. σ, α, u, and the coordination situation of lithium ions are summarized in Fig. 5 and Table S3 (ESI†). In this section, σ and u represent the conductivity and mobility of lithium ions, respectively.

For SLIC-SPEs without spacers, with n increasing from 1 to 11, σ decreased from 0.184 mS cm^{-1} to almost zero (Fig. 5a), which is similar to the ionic conductivity of polyionic liquids.[70,72] α decreased from 68% to 19%, and more associative clusters were produced. In LiEtTFSI and (LiEtTFSI)$_2$, lithium ions exist individually without forming large clusters (Fig. 5c and e), while in (LiEtTFSI)$_4$ and (LiEtTFSI)$_{11}$, large cation–anion clusters formed and contained about 35 and 47 lithium ions, respectively (Fig. 5c, f and g).

Unlike the monomer salts in Section 3.2, where u only varies a little. u decreases significantly from 2.72×10^{-6} cm^2 V^{-1} s^{-1} to almost zero with the decrease in α. The result shows that in polyanions, α and u determine the conductivity together. When $n > 2$, the u decreases sharply, causing σ to almost zero, even when α still accounts for about 10%. This phenomenon may be associated with the formation of large cation–anion clusters. After the formation of these large clusters, the background charges of the anions were confined within the clusters and could not undergo local relaxation with the movement of
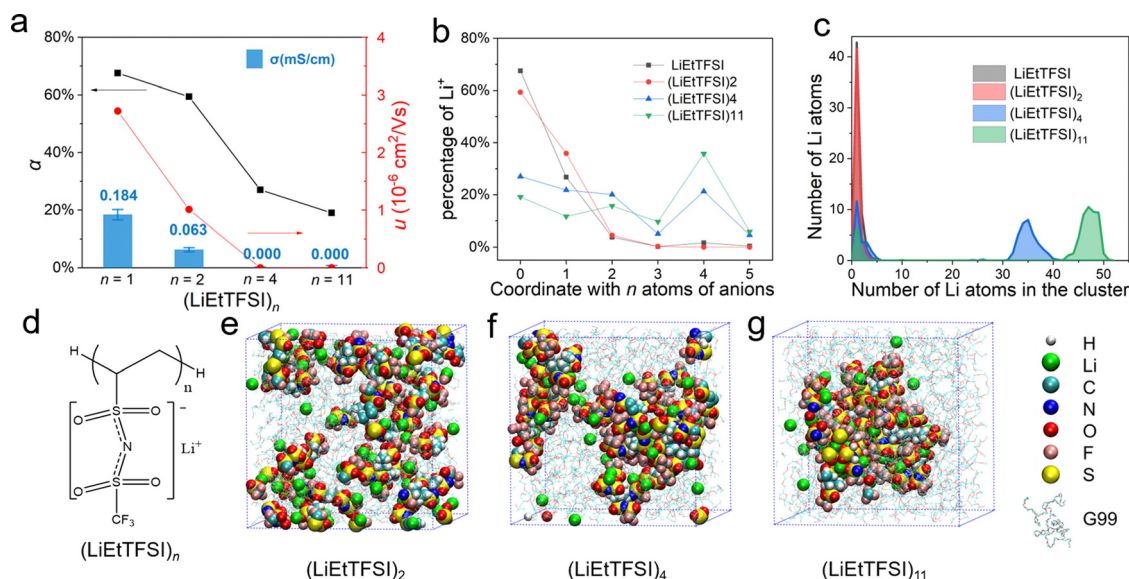
Fig. 5 The simulation results of (LiEtTFSI)$_n$ in G99 electrolyte with O/Li = 20 at 80 °C. (a) σ, α, and u of lithium ions. (b) Percentage of Li$^+$ coordinated with N atoms of anions. (c) Number and size of cation–anion clusters. (e) Structural formula of the electrolyte. (e)–(g) Snapshots of simulation boxes.

cations, which leads to an increase in the migration energy barrier of lithium ions.

To investigate the effect of different anion spacers in polyanions, (LiEtTFSI-PE$_2$)$_{11}$, (LiEtTFSI-PE$_4$)$_{11}$, and (LiEtTFSI-PE$_8$)$_{11}$ were constructed. The σ, α, and u of lithium ions are summarized in Fig. 6.

For SLIC-SPEs with different spacers, large cation–anion clusters disappear (Fig. 6c). σ firstly rises sharply from zero ($m = 0$) to 0.059 mS cm^{-1} ($m = 4$) and then slightly decreases to 0.046 mS cm^{-1} ($m = 8$) (Fig. 6a). α increased from 19% to 60%

(Fig. 6a and b), while u rises first from zero ($m = 0$) to 1.08 × 10^{-6} cm^2 V^{-1} s^{-1} ($m = 4$) and then slightly reduces to 0.95 × 10^{-6} cm^2 V^{-1} s^{-1} ($m = 8$). In other words, when the spacers between anions are large enough, α increases to almost the same as the monomer lithium salts; however, u cannot reach the same level of monomer lithium salts but only 40% of that. Through the trends of α and u, the reasons for changes in the two factors could be speculated. α is mainly affected by the concentration of negative charge due to the aggregation of anionic groups as α gradually decreases while n increases from
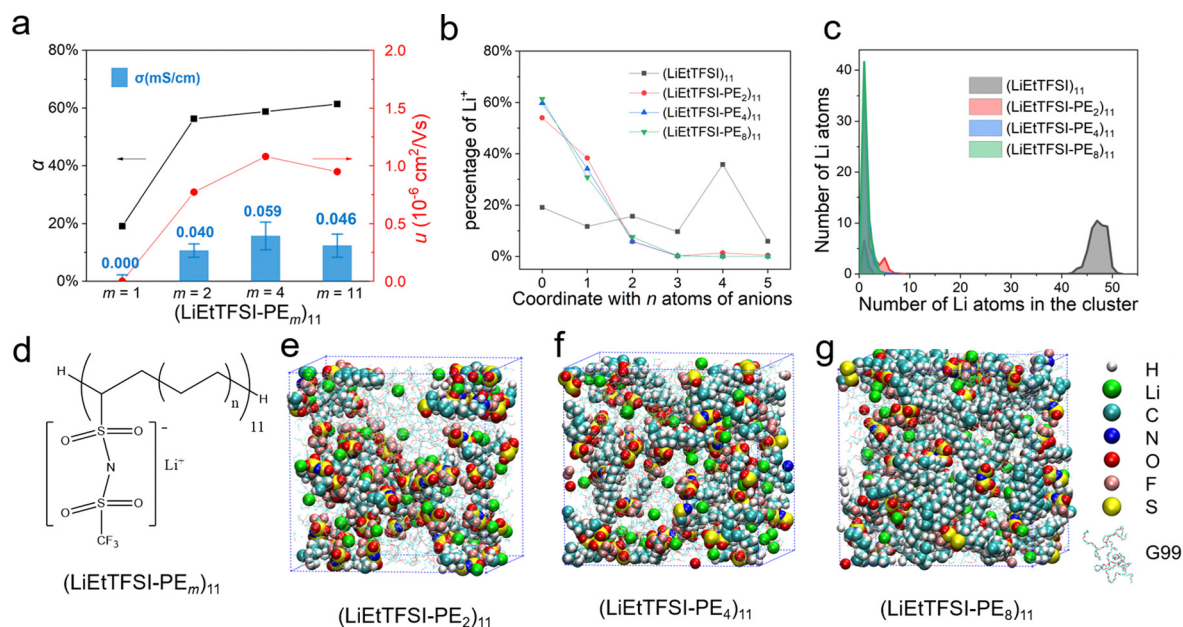
Fig. 6 The simulation results of (LiEtTFSI-PE$_m$)$_{11}$ in G99 electrolyte with O/Li = 20 at 80 °C. (a) σ, α, and u of lithium ions. (b) Percentage of Li$^+$ coordinated with N atoms of anions. (c) Number and size of cation–anion clusters. (d) Structural formula of the electrolyte. (e)–(g) Snapshots of the simulation boxes.

This journal is © the Owner Societies 2023

Phys. Chem. Chem. Phys., 2023, **25**, 29894–29904 | **29901**

1 to 11 without spacers and returns to the level of monomer salts with enlarging spacers. However, u can only reach 40% of the monomer salts at the same time. This could be due to the local relaxation capacity of the anion groups, which affects the energy barrier for the migration of lithium ions. The anions are fixed to the polymer chain, and their local movements are still restricted although lithium ions have been largely dissociated. The restriction may share similarities with the confinement of anions, resulting from the formation of large cation–anion clusters in $(LiEtTFSI)_{11}$, although the extent of restriction may vary. We will delve deeper into the impact of anion confinement on conductivity in our future work.

When replacing G99 with G4, the results show that the trends of σ, α, and u are similar (Table S6 and Fig. S14, ESI†), which indicates that the influence of anion relaxation effects on the migration energy barriers exists in both macromolecular and small molecules solvents. For exploring the influence of the anionic group on the σ of the polyanion, the EtTFSI group was replaced by $EtSO_3$ with weaker dissociation ability. The general formula is $(LiEtSO_3-PE_m)_n$. The results in Fig. S15 and Table S7 (ESI†) show that all σ is close to zero. Although the fitted σ is 0.032 mS cm^{-1} for $n = 11$ and $m = 8$, the big jitter of the drift curve makes the value unreliable (Fig. S15a, ESI†). α and u are close to zero, and all ions are almost gathered into a cluster (Fig. S15d–g, ESI†). The results show that the polymer composed of lithium salt monomer, which is hard to dissociate, would have poor conductivity even with large spacers between the anion groups. It indicates that the anionic group having a good dissociation capability is a prerequisite for high conductivity SLIC-SPEs.

In summary, for polyanions, both α and u are crucial factors influencing σ; however, u has a more significant impact. Polymerization causes a decrease in α and u, while spacers between anion groups increase the α and u. When the spacers are large enough, α can reach the level of monomer salts, but u can only reach 40% of that. The change in α results from the negative charge concentration, while the change in u stems from the local relaxation ability of anionic groups. Therefore, appropriate spacers can substantially enhance the conductivity of polyanions. However, there remains considerable room for improvement in u. Designing a flexible main chain to reduce the migration energy barrier of lithium ions may further enhance u.

4. Conclusions

In this work, a simulation method that has quantitative accuracy matching experiments was utilized to investigate the conducting behaviors of single lithium-ion conducting solid polymer electrolytes (SLIC-SPEs) dispersed in polyethylene oxide (PEO) matrix. The method was based on molecular dynamics simulation with OPLS-AA force field. The conductivities of several lithium salts were measured to optimize the scale factor of atomic charges n_s. All conductivities were simulated by counting the drift current of ions under an electric field, which shows better agreement with experimental data than calculating the conductivities solely from the diffusion coefficient.

The influence of anionic and main chain structures on the conductivities of SLIC-SPEs were studied using a model that includes three components: an R1 intermediate group, an R2 end group, and an R3 main chain. The anionic group was manipulated by altering R1 and R2, while the main chain was adjusted by varying the length of the chain and the spacers between the anionic groups. For different anionic groups, the dissociation degree is the primary factor that determines conductivity. Increasing the size of R1 does not always result in a monotonically increase in the conductivity and dissociation degree; instead, the maximum value is reached when R1 = $-(SO_2)N(SOCF_3)N(SO_2)-$. At the same time, the reduction stability is decreased when increasing the size of R1. R2 with higher electron-withdrawing ability could enhance the conductivity, but its effect was relatively minor in comparison with that of R1. Meanwhile, R2 with conjugate effect such as $-Ph$ and $-NO_2$ leads to weak reduction stability. Hence, the design strategy for the anionic group is to achieve a balance between conductivity and reduction stability. An R1 with moderate size and an R2 with electron-withdrawing inductive effect may be an equilibrium strategy. In terms of different R3 structures, both dissociation degree and mobility are significant factors in conductivity, with mobility being more influential. When lithium salts were polymerized without spacers, both dissociation degree and mobility decreased, resulting in the conductivity dropping to zero. Nevertheless, increasing the spacers between the anions restored the dissociation degree to the level of monomer salts but only enabled the mobility to reach approximately 40%, which is possibly attributable to the restricted local relaxation ability of the anionic group.

In order to enhance the conductivities of SLIC-SPEs, two primary strategies are commonly employed: improving the structure of the anionic group to increase the dissociation degree or enhancing the main chain structure of polyanions to boost the mobility. For anionic groups that are hard to dissociate such as $-SO_3$, improving the structure of the anionic group can lead to a substantial increase in the conductivity by several orders of magnitude, but modifications to the chain structure are less effective. However, if anionic groups are easy to dissociate, such as $-(SO_2)N(SO_2)CF_3$, increasing the mobility provides more significant room for improvement. When controlling the anionic structure, the conductivity could be raised by approximately 45% at the cost of a reduction in the stability, while controlling the main chain structure could decrease the migration energy barrier of lithium ions, resulting in an increase in the conductivity of up to 250%. After reflecting on these findings, it is worth noting that, at the present stage of the SLIC-SPEs research, it may be more promising to elevate the mobility by rationally designing the structure of the polymer main chain.

Conflicts of interest

The authors declare that they have no known competing financial interests or personal relationships that could have appeared to influence the work reported in this paper.

29902 | *Phys. Chem. Chem. Phys.*, 2023, **25**, 29894–29904

This journal is © the Owner Societies 2023

Acknowledgements

References

1 H. Zhang, C. M. Li, M. Piszcz, E. Coya, T. Rojo, L. M. Rodriguez-Martinez, M. Armand and Z. B. Zhou, *Chem. Soc. Rev.*, 2017, **46**, 797–815.

2 X.-B. Cheng, R. Zhang, C.-Z. Zhao and Q. Zhang, *Chem. Rev.*, 2017, **117**, 10403–10473.

3 K. Matsumoto, K. Inoue, K. Nakahara, R. Yuge, T. Noguchi and K. Utsugi, *J. Power Sources*, 2013, **231**, 234–238.

4 K. Xu, *Chem. Rev.*, 2014, **114**, 11503–11618.

5 Y. L. Yan-Yan Zhang, Yi-Ming Lu, Pei-Ping Yu, Wen-Xuan Du, Bing-Yun Ma, Miao Xie, Hao Yang and Tao Cheng, *J. Electrochem.*, 2022, **28**, 2105181.

6 S.-W. Ryu, P. E. Trapa, S. C. Olugebefola, J. A. Gonzalez-Leon, D. R. Sadoway and A. M. Mayes, *J. Electrochem. Soc.*, 2005, **152**, A158–A163.

7 H.-T. Kim and J.-K. Park, *Polym. Bull.*, 1996, **36**, 427–433.

8 X. Shen, P. Zhang, H. Li, R. Li, X. Wang, H. Hua, B. Huang, J. Yang and J. Zhao, *Aerospace Shanghai (Chinese & English)*, 2020, **37**, 13–22.

9 F. Ahmed, I. Choi, M. M. Rahman, H. Jang, T. Ryu, S. Yoon, L. Jin, Y. Jin and W. Kim, *ACS Appl. Mater. Interfaces*, 2019, **11**, 34930–34938.

10 P.-Y. Ji, J. Fang, Y.-Y. Zhang, P. Zhang and J. Zhao, *ChemElectroChem*, 2017, **4**, 2352–2358.

11 K. Jeong, S. Park, G. Y. Jung, S. H. Kim, Y. H. Lee, S. K. Kwak and S. Y. Lee, *J. Am. Chem. Soc.*, 2019, **141**, 5880–5885.

12 N. Shubha, H. J. Zhu, M. Forsyth and M. Srinivasan, *Polymer*, 2016, **99**, 748–755.

13 X. Shen, H. Hua, H. Li, R. Li, T. Hu, D. Wu, P. Zhang and J. Zhao, *Polymer*, 2020, **201**, 122568.

14 H. Li, X. Shen, H. Hua, J. Gao, Z. Wen, X. Wang, L. Peng, D. Wu, P. Zhang and J. Zhao, *Solid State Ionics*, 2020, **347**, 115246.

15 C. Cao, Y. Li, Y. Y. Feng, P. Long, H. R. An, C. Q. Qin, J. K. Han, S. W. Li and W. Feng, *J. Mater. Chem. A*, 2017, **5**, 22519–22526.

16 H. D. Nguyen, G. T. Kim, J. L. Shi, E. Paillard, P. Judeinstein, S. Lyonnard, D. Bresser and C. Iojoiu, *Energy Environ. Sci.*, 2018, **11**, 3298–3309.

17 Y. Z. Chen, Y. S. Tian, Z. Li, N. Zhang, D. L. Zeng, G. D. Xu, Y. F. Zhang, Y. B. Sun, H. Z. Ke and H. S. Cheng, *J. Membr. Sci.*, 2018, **566**, 181–189.

18 L. Porcarelli, A. S. Shaplov, M. Salsamendi, J. R. Nair, Y. S. Vygodskii, D. Mecerreyes and C. Gerbaldi, *ACS Appl. Mater. Interfaces*, 2016, **8**, 10350–10359.

19 Q. Ma, H. Zhang, C. W. Zhou, L. P. Zheng, P. F. Cheng, J. Nie, W. F. Feng, Y. S. Hu, H. Li, X. J. Huang, L. Q. Chen, M. Armand and Z. B. Zhou, *Angew. Chem., Int. Ed.*, 2016, **55**, 2521–2525.

20 H. Y. Yuan, J. Y. Luan, Z. L. Yang, J. Zhang, Y. F. Wu, Z. G. Lu and H. T. Liu, *ACS Appl. Mater. Interfaces*, 2020, **12**, 7249–7256.

21 J. H. Baik, S. Kim, D. G. Hong and J. C. Lee, *ACS Appl. Mater. Interfaces*, 2019, **11**, 29718–29724.

22 R. Meziane, J.-P. Bonnet, M. Courty, K. Djellab and M. Armand, *Electrochim. Acta*, 2011, **57**, 14–19.

23 Q. Ma, Y. Xia, W. Feng, J. Nie, Y.-S. Hu, H. Li, X. Huang, L. Chen, M. Armand and Z. Zhou, *RSC Adv.*, 2016, **6**, 32454–32461.

24 Y. S. Zhu, X. W. Gao, X. J. Wang, Y. Y. Hou, L. L. Liu and Y. P. Wu, *Electrochem. Commun.*, 2012, **22**, 29–32.

25 Y. S. Zhu, X. J. Wang, Y. Y. Hou, X. W. Gao, L. L. Liu, Y. P. Wu and M. Shimizu, *Electrochim. Acta*, 2013, **87**, 113–118.

26 Y. Zhang, R. Rohan, Y. Sun, W. Cai, G. Xu, A. Lin and H. Cheng, *RSC Adv.*, 2014, **4**, 21163–21170.

27 X. J. Wang, Z. H. Liu, Q. S. Kong, W. Jiang, J. H. Yao, C. J. Zhang and G. L. Cui, *Solid State Ionics*, 2014, **262**, 747–753.

28 G. Xu, Y. Sun, R. Rohan, Y. Zhang, W. Cai and H. Cheng, *J. Mater. Sci.*, 2014, **49**, 6111–6117.

29 B. Qin, Z. Liu, J. Zheng, P. Hu, G. Ding, C. Zhang, J. Zhao, D. Kong and G. Cui, *J. Mater. Chem. A*, 2015, **3**, 7773–7779.

30 X. Wang, J. Sun, C. Feng, X. Wang, M. Xu, J. Sun, N. Zhang, J. Ma, Q. Wang, C. Zong and G. Cui, *J. Energy Chem.*, 2021, **55**, 228–235.

31 H. Yuan, J. Luan, Z. Yang, J. Zhang, Y. Wu, Z. Lu and H. Liu, *ACS Appl. Mater. Interfaces*, 2020, **12**, 7249–7256.

32 S. Feng, D. Shi, F. Liu, L. Zheng, J. Nie, W. Feng, X. Huang, M. Armand and Z. Zhou, *Electrochim. Acta*, 2013, **93**, 254–263.

33 R. Li, H. Hua, Y. Zeng, J. Yang, Z. Chen, P. Zhang and J. Zhao, *J. Energy Chem.*, 2022, **64**, 395–403.

34 C. Park, M. Kanduč, R. Chudoba, A. Ronneburg, S. Risse, M. Ballauff and J. Dzubiella, *J. Power Sources*, 2018, **373**, 70–78.

35 K. Shigenobu, M. Shibata, K. Dokko, M. Watanabe, K. Fujii and K. Ueno, *Phys. Chem. Chem. Phys.*, 2021, **23**, 2622–2629.

36 K. J. Lin and J. K. Maranas, *Phys. Chem. Chem. Phys.*, 2013, **15**, 16143–16151.

37 K. Shimizu, A. A. Freitas, R. Atkin, G. G. Warr, P. A. FitzGerald, H. Doi, S. Saito, K. Ueno, Y. Umebayashi, M. Watanabe and J. N. Canongia Lopes, *Phys. Chem. Chem. Phys.*, 2015, **17**, 22321–22335.

38 S. Tsuzuki, W. Shinoda, M. Matsugami, Y. Umebayashi, K. Ueno, T. Mandai, S. Seki, K. Dokko and M. Watanabe, *Phys. Chem. Chem. Phys.*, 2015, **17**, 126–129.

39 O. Borodin and G. D. Smith, *Macromolecules*, 2006, **39**, 1620–1629.

40 D. Diddens, A. Heuer and O. Borodin, *Macromolecules*, 2010, **43**, 2028–2036.

41 A. Maitra and A. Heuer, *Phys. Rev. Lett.*, 2007, **98**, 227802.

42 H. Hua, X. Yang, P. Zhang and J. Zhao, *J. Phys. Chem. C*, 2023, **127**, 17324–17334.

43 N. Meng, F. Lian and G. Cui, *Small*, 2021, **17**, 2005762.

44 A. V. Marenich, J. Ho, M. L. Coote, C. J. Cramer and D. G. Truhlar, *Phys. Chem. Chem. Phys.*, 2014, **16**, 15068–15106.

45 J. B. Le, A. Chen, L. Li, J. F. Xiong, J. Lan, Y. P. Liu, M. Iannuzzi and J. Cheng, *J. Am. Chem. Soc.*, 2021, **1**, 569–577.

46 J.-B. Le and J. Cheng, *Curr. Opin. Electrochem.*, 2021, **27**, 100693.

47 S. O. Nielsen, R. E. Bulo, P. B. Moore and B. Ensing, *Phys. Chem. Chem. Phys.*, 2010, **12**, 12401–12414.

48 X. H. Yang, Y. B. Zhuang, J. X. Zhu, J. B. Le and J. Cheng, *WIREs Comput. Mol. Sci.*, 2021, **12**, e1559.

49 S. Chowdhuri and A. Chandra, *J. Chem. Phys.*, 2001, **115**, 3732–3741.

50 K.-H. Shen and L. M. Hall, *Macromolecules*, 2020, **53**, 3655–3668.

51 M. J. Frisch, G. W. Trucks, H. B. Schlegel, G. E. Scuseria, M. A. Robb, J. R. Cheeseman, G. Scalmani, V. Barone, B. Mennucci, G. A. Petersson, H. Nakatsuji, M. Caricato, X. Li, H. P. Hratchian, A. F. Izmaylov, J. Bloino, G. Zheng, J. L. Sonnenberg, M. Hada, M. Ehara, K. Toyota, R. Fukuda, J. Hasegawa, M. Ishida, T. Nakajima, Y. Honda, O. Kitao, H. Nakai, T. Vreven, J. A. Montgomery, Jr, J. E. Peralta, F. Ogliaro, M. Bearpark, J. J. Heyd, E. Brothers, K. N. Kudin, V. N. Staroverov, R. Kobayashi, J. Normand, K. Ragha-vachari, V. N. Staroverov, R. Kobayashi, J. Normand, K. Raghavachari, A. Rendell, J. C. Burant, S. S. Iyengar, J. Tomasi, M. Cossi, N. Rega, N. J. Millam, M. Klene, J. E. Knox, J. B. Cross, V. Bakken, C. Adamo, J. Jaramillo, R. Gomperts, R. E. Stratmann, O. Yazyev, A. J. Austin, R. Cammi, C. Pomelli, J. W. Ochterski, R. L. Martin, K. Morokuma, V. G. Zakrzewski, G. A. Voth, P. Salvador, J. J. Dannenberg, S. Dapprich, A. D. Daniels, Ö. Farkas, J. Foresman, J. V. B. Ortiz, J. Cioslowski and D. J. Fox, *Gaussian 09, Revision E.01*, Gaussian, Inc., Wallingford CT, 2013.

52 P. J. Stephens, F. J. Devlin, C. F. Chabalowski and M. J. Frisch, *J. Phys. Chem.*, 1994, **98**, 11624–11627.

53 R. Krishnan, J. S. Binkley, R. Seeger and J. A. Pople, *J. Chem. Phys.*, 1980, **72**, 650–654.

54 S. Grimme, J. Antony, S. Ehrlich and H. Krieg, *J. Chem. Phys.*, 2010, **132**, 154104.

55 C. I. Bayly, P. Cieplak, C. Wendy and P. A. Kollman, *J. Phys. Chem.*, 1993, **97**, 10269.

56 T. Lu and F. Chen, *J. Comput. Chem.*, 2012, **33**, 580–592.

57 J. Zhang and T. Lu, *Phys. Chem. Chem. Phys.*, 2021, **23**, 20323–20328.

58 W. Humphrey, A. Dalke and K. Schulten, *J. Mol. Graphics*, 1996, **14**(33–38), 27–38.

59 M. J. Abraham, T. Murtola, R. Schulz, S. Páll, J. C. Smith, B. Hess and E. Lindahl, *SoftwareX*, 2015, **1–2**, 19–25.

60 W. L. Jorgensen, D. S. Maxwell and J. TiradoRives, *J. Am. Chem. Soc.*, 1996, **118**, 11225–11236.

61 M. L. P. Price, D. Ostrovsky and W. L. Jorgensen, *J. Comput. Chem.*, 2001, **22**, 1340–1352.

62 A. A. Teran, M. H. Tang, S. A. Mullin and N. P. Balsara, *Solid State Ionics*, 2011, **203**, 18–21.

63 J. Shi and C. A. Vincent, *Solid State Ionics*, 1993, **60**, 11–17.

64 P. M. Anderson and M. R. Wilson, *Mol. Phys.*, 2005, **103**, 89–97.

65 A. W. S. d Silva and W. F. Vranken, *BMC Res. Notes*, 2012, **5**, 367.

66 L. Martinez, R. Andrade, E. G. Birgin and J. M. Martinez, *J. Comput. Chem.*, 2009, **30**, 2157–2164.

67 B. Hess, *J. Chem. Phys.*, 2002, **116**, 209–217.

68 C. Calero, J. Faraudo and M. Aguilella-Arzo, *Mol. Simul.*, 2011, **37**, 123–134.

69 N. J. English and C. J. Waldron, *Phys. Chem. Chem. Phys.*, 2015, **17**, 12407–12440.

70 J. R. Keith, S. Mogurampelly, F. Aldukhi, B. K. Wheatle and V. Ganesan, *Phys. Chem. Chem. Phys.*, 2017, **19**, 29134–29145.

71 H. Ohno, M. Yoshizawa and W. Ogihara, *Electrochim. Acta*, 2004, **50**, 255–261.

72 H. Ohno, *Electrochim. Acta*, 2001, **46**, 1407–1411.